PET imaging of TSPO in a rat model of local neuroinflammation induced by intracerebral injection of lipopolysaccharide.

Ory D, Planas A, Dresselaers T, Gsell W, Postnov A, Celen S, Casteels C, Himmelreich U, Debyser Z, Van Laere K, Verbruggen A, Bormans G.

Published in: Nucl Med Biol. 2015 Oct;42(10):753-61.

doi: 10.1016/j.nucmedbio.2015.06.010

PET imaging of TSPO in a rat model of local neuroinflammation induced by intracerebral injection of lipopolysaccharide

Dieter Ory[a], Anna Planas[b], Tom Dresselaers[c], Willy Gsell[c], Andrey Postnov[d], Sofie Celen[a], Cindy Casteels[d], Uwe Himmelreich[c], Zeger Debyser[e], Koen Van Laere[d], Alfons Verbruggen[a], Guy Bormans[a]

[a] Laboratory for Radiopharmacy, Department of Pharmaceutical and Pharmacological Sciences, KU Leuven, Leuven, Belgium
[b] Department of Brain Ischemia and Neurodegeneration, Institute for Biomedical Research, Barcelona, Spain
[c] Biomedical MRI, Department of Imaging and Pathology, KU Leuven, Leuven, Belgium
[d] Nuclear Medicine and Molecular Imaging, University Hospital and KU Leuven, Leuven, Belgium
[e]Laboratory for Molecular Virology and Gene Therapy, Department of Pharmaceutical and Pharmacological Sciences, KU Leuven, Leuven, Belgium

Address for correspondence:

Prof. Guy Bormans, Laboratory for Radiopharmacy, Campus Gasthuisberg O&N2, Herestraat 49 Box 821, BE-3000 Leuven, Belgium. Phone: +32 16 330447; Fax: +32 16 330449; E-mail address: Guy.Bormans@pharm.kuleuven.be

Key words: neuroinflammation, [^{18}F]DPA-714, PET, lipopolysaccharide

Abbreviated title: Characterization of LPS model

Objective: The goal of this study was to measure functional and structural aspects of local neuroinflammation induced by intracerebral injection of lipopolysaccharide (LPS) in rats using TSPO microPET imaging with [^{18}F]DPA-714, magnetic resonance imaging (MRI), *in vitro* autoradiography and immunohistochemistry (IHC) in order to characterize a small animal model for screening of new PET tracers targeting neuroinflammation.

Methods: Rats were injected stereotactically with LPS (50 μg) in the right striatum and with saline in the left striatum. [^{18}F]DPA-714 microPET, MRI, *in vitro* autoradiography and IHC studies were performed at different time points after LPS injection for 1 month.

Results: Analysis of the microPET data demonstrated high uptake of the tracer in the LPS injected site with an affected-to-non-affected side binding potential ratio ($BP_{right\text{-}to\text{-}left}$) of 3.0 at 3 days after LPS injection. This BP ratio decreased gradually over time to 0.9 at 30 days after LPS injection. *in vitro* autoradiography ([^{18}F]DPA-714) and IHC (CD68, GFAP and TSPO) confirmed local neuroinflammation in this model. Dynamic contrast enhanced (DCE) MRI demonstrated BBB breakdown near the LPS injection site at day 1, which gradually resolved over time and was absent at 1 month after LPS injection.

Conclusion: The LPS model is useful for first screening of newly developed tracers because of the easy design and the robust, unilateral inflammatory reaction allowing the use of the contralateral region as control. Additionally, this model can be used to test and follow up the benefits of anti-inflammatory therapies by non-invasive imaging.

1. Introduction

Neuroinflammation is the inflammation associated to with central nervous system (CNS) pathologies including Parkinson's disease (PD), Alzheimer's disease (AD), stroke, multiple sclerosis (MS), amyotrophic lateral sclerosis (ALS), Huntington's disease (HD), viral/bacterial infection, neoplasia and head trauma. These diseases trigger a cerebral immune activation which can lead to both collateral damage to brain tissue as well as neuroregeneration [1]. Microglia are resident CNS cells that have phenotypic similarities and functions to macrophages and constitute up to 10% of the total cell population of the brain. Microglia are plastic cells that show phenotypic changes in response to environmental signals, and can exert either neuroprotective or neurotoxic roles depending on the context.

The most studied imaging biomarker of neuroinflammation is the translocator protein (TSPO) [2] receptor or peripheral benzodiazepine receptor (PBR) that is expressed on the outer mitochondrial membrane of microglia and macrophages [3]. TSPO plays a crucial role in neurosteroidogenesis important during brain development and normal functioning during adulthood [3]. In the central nervous system, TSPO expression is low under healthy circumstances. However, in response to neuronal insults, TSPO expression increases mainly in microglia and astrocytes as detected in several neurodegenerative diseases such as PD, ALS, HD and AD [3]. The role of TSPO in regulation of neuroinflammation still remains to be elucidated. While TSPO antagonists can attenuate inflammation, a recent study of Bae et al. [4] suggested that TSPO is a negative regulator of neuroinflammation in microglia. TSPO has been identified as a valuable imaging biomarker for neuroinflammation since the degree of TSPO upregulation in response to injury is correlated with the degree of damage in neuroinflammation [5]. [^{18}F]DPA-714 is a specific radiotracer for TSPO and has already been successfully evaluated in several animal models of neuroinflammation [6–8], in healthy humans [9] and ALS patients [10]. Recently, Owen *et al*. [11] reported a human TSPO polymorphism with a trimodal distribution in binding affinity (high-affinity, low-affinity and mixed affinity binders) for several TSPO ligands. The consequence of this polymorphism is that knowledge of binding status is needed to correctly quantify TSPO expression using these PET ligands in humans [11]. In the present

study, we used [^{18}F]DPA-714 to characterize TSPO expression in a rat model of acute, local neuroinflammation induced by lipopolysaccharide (LPS). LPS is found in the outer membrane of gram-negative bacteria and activates Toll-like-receptor 4 (TLR4) mainly expressed by microglia and macrophages. TLR4 activation induces signal transduction pathways that regulate diverse transcriptional and posttranscriptional processes involved in inflammation [12]. Moon et al. [13] used the LPS model to compare [^{11}C]PBR28 with their newly synthesized [^{18}F]fluoromethyl-PBR28, while Dickens et al. [14] used the LPS model to compare [^{11}C]PK11195 and [^{18}F]GE-180. However, only one time point after LPS injection was studied to compare different TSPO tracers in these previous reports. The goal of the current study was to fully characterize the LPS rat model longitudinally with an established neuroinflammation tracer [^{18}F]DPA-714, magnetic resonance imaging (MRI) and immunohistochemistry (IHC) to assess the dynamics of the neuroinflammatory reaction. This model will be used for screening of newly developed PET radiotracers as putative biomarkers of neuroinflammation.

2. Material and methods

a. LPS-induced neuroinflammation rat model

An acute rat model of neuroinflammation was developed using lipopolysaccharide (LPS; E. Coli 055:B5; Sigma Aldrich, St. Louis, MO, USA). Female Wistar rats (250 - 300 g; 2 months old) were kept under gas anesthesia (2.5% isoflurane in O_2 at a flow rate of 1 L/min) and positioned in a stereotactic head frame (Stoelting, Wood Dale, IL, USA). A small hole was drilled in the skull at the appropriate location using Bregma as reference. Neuroinflammation was induced by injecting 50 μg LPS dissolved in 4 μl of sterile NaCl 0.9% at the following coordinates: +0.5 mm antero-posterior, 3 mm lateral (right hemisphere), 5.5/4.5 mm dorsoventral. After injection of 2 μl, the needle was retracted for 1 mm dorsoventral and another 2 μl was injected. The needle was left in place for an additional 10 min before being slowly withdrawn from the brain. The contralateral side was injected as control with 4 μl of sterile 0.9% NaCl solution. Animals (N=27) were housed in individually

ventilated cages in a thermoregulated (~22 °C), humidity-controlled facility under a 12 h/12 h light/dark cycle with access to food and water ad libitum. All animal experiments were conducted according to the Belgian code of practice for the care and use of animals, after approval from the local University Ethics Committee for Animals.

b. Experimental design

The experimental design is summarized in figure 1. MicroPET and MRI studies were performed on 1, 3, 7 and 30 days after LPS injection. *In vitro* autoradiography and IHC were performed on 1, 4, 8 and 31 days after LPS injection. There is a difference of 1 day between the *in vivo* and *in vitro* experiments because from the animals that were scanned (PET and MRI) on 3, 7 and 30 days after LPS injection, one animal was sacrificed 1 day later, respectively on day 4, 8 and 31, for *in vitro* autoradiography and IHC to verify microglial proliferation and TSPO expression in the same animal. In that manner the fluorine-18 was sufficiently decayed and brain slices could be made. On day 1 after LPS injection we did not observe significant retention of [^{18}F]DPA-714 in the ipsilateral site in the microPET study and therefore we sacrificed the animals at day 1 after LPS injection for *in vitro* autoradiography and IHC. To increase N for *in vitro* autoradiography and IHC, additional animals were injected with LPS and sacrificed on day 1, 4, 8 and 31 after LPS injection for *in vitro* autoradiography and IHC ($N \geq 3$ for each time point and each experiment; Figure 1). IHC and *in vitro* autoradiography were performed on adjacent brain slices. Additionally, a pre-treatment study (PK11195 10 mg/kg subcutaneously 60 min before tracer injection; N=3) and a displacement study (PK11195 5 mg/kg intravenously 30 min after tracer injection; N=3) were performed at 3 days after LPS injection. All statistical studies were performed with the unpaired two-tailed t-test, a p value less than 0.05 was considered statistically significant. Calculations were carried out using GraphPad Prism v5.0 (San Diego, CA).

Figure 1

c. Radiosynthesis

The radiotracer [^{18}F]DPA-714 was synthesized as previously described [15] with some small modifications: most importantly, the semi-preparative HPLC purification was performed using an ethanol based mobile phase, EtOH:NH_4OAc 10 mM pH 7 35:65 V/V. The final preparation containing less than 10% of EtOH was sterile filtered through a 0.22-μm membrane filter (Millex®-GV, Millipore, Billerica, USA). [^{18}F]DPA-714 (> 98% radiochemically pure) was obtained with 45-60% yield (relative to starting [^{18}F]F^- radioactivity). The specific activity at end of synthesis ranged from 56 to 148 GBq/μmol. Precursor and reference compound were kindly provided by Prof. Michael Kassiou (University of Sydney, Australia).

d. microPET

Imaging experiments were performed on a Focus 220 microPET scanner (Concorde Microsystems, Knoxville, TN, USA). Rats were injected with about 74 MBq of [^{18}F]DPA-714 via a tail vein (volume injected <1 mL; specific activity at injection: 51-130 GBq/μmol). During all PET sessions, animals were kept under gas anesthesia (2.5% isoflurane in O_2 at a flow rate of 1 L/min). List-mode 120-min microPET scans were acquired. Acquisition data were then Fourier rebinned in 27 time frames (4 x 15 s, 4 x 60 s, 5 x 180 s, 8 x 300 s, 6 x 600 s) and reconstructed using maximum a posteriori iterative reconstruction. The images were spatially aligned to a rat brain [^{18}F]FDG template in Paxinos coordinates [16] using an affine transformation, allowing the use of a predefined volumes of interest map. Time-activity curves (TAC) were generated for right and left striatum for each individual scan using PMOD software (version 3.2; PMOD technologies, Zurich, Switzerland).

Kinetic modeling based on simplified reference tissue model (SRTM) [17] with the contralateral (left) striatum as a reference region was performed to quantify the uptake difference between the right and the left striatum.

e. *In vitro* autoradiography

The rats were sacrificed, brain was removed, rinsed with saline to remove blood, rapidly frozen in 2-methylbutane (-40 °C) and stored at -20 °C for 24 h. Transversal sections from the brain were obtained using a cryotome (Shandon cryotome FSE; Thermo Fisher, Waltham, USA), mounted on adhesive microscope slides (Superfrost Plus; Thermo Fisher) and stored at -20 °C until autoradiography was performed. Brain slices were dried and preincubated in 50 mM tris-HCl buffer (pH 7.4) for 10 min at room temperature. Before incubation with [^{18}F]DPA-714, the brain sections were dried. The brain sections were incubated with 590 kBq of tracer for 10 min. The brain sections were washed twice for 10 min in 50 mM tris-HCl (pH 7.4) + 0.3% BSA buffer at 4 °C. After a quick dip in water at 4 °C, the slides were dried. Autoradiograms were obtained by exposing the slides for 5 min to a high performance phosphor storage screen (super-resolution screen; Perkin Elmer, Waltham, USA). The screens were read using a Cyclone Plus system (Perkin Elmer) and analyzed using Optiquant software (Perkin Elmer). The radioactivity concentration in the autoradiograms is expressed in digital light units (DLU)/mm^2 corrected for background. The data were processed as right striatum (LPS) to left striatum (saline) ratios (DLU/mm^2 in right striatum divided by DLU/mm^2 in left striatum).

f. Immunohistochemistry for TSPO and CD68

Cryostat brain sections (adjacent to the slices used for *in vitro* autoradiography) were fixed with ethanol, blocked with normal serum and incubated overnight at 4 ºC with a rabbit polyclonal primary antibody against TSPO (#NBP1-45769 from Novus Biologicals, Littleton, USA) diluted 1:100. Then, sections were incubated for 2 h at room temperature with a secondary anti-rabbit antibody (Alexa Fluor-488, Molecular Probes, Eugene, USA). Double immunostaining was carried out with mouse monoclonal antibodies against the microglia/macrophage marker CD68 (ED1, #MCA341R, Serotec, Kidlington, Oxford) diluted 1:100 or the astroglia marker glial fibrillary acidic protein (GFAP, #G3893, Sigma) followed by a secondary anti-mouse antibody (Alexa Fluor-546,

190 Molecular Probes). Sections were counterstained with To-Pro3 (Invitrogen, Carlsbad, USA) to
191 visualize the cell nuclei. They were mounted in Mowiol 488 (Sigma–Aldrich) and were observed in a
192 confocal microscope (Leica TCS, SPC, Wetzlar, Germany).

193

194 g. Magnetic resonance imaging (MRI)

195 MR images were recorded on a 9.4T/200 Biospec small animal MR system (Bruker Biospin,
196 Ettlingen, Germany) equipped with a 117-mm inner diameter actively shielded gradient set of 600
197 mT/m using a 7-cm linearly polarized resonator for transmission and an actively-decoupled dedicated
198 rat brain surface coil for receiving (Bruker Biospin). Rats were anesthetized with isoflurane in oxygen,
199 their respiration monitored and body temperature controlled at 37 °C using a water heating circuit (SA
200 Instruments, Stony Brook, NY, USA). The following MR images were recorded before contrast
201 injection: (1) 3-dimensional T_2-weighted (rapid acquisition with relaxation enhancement, RARE, echo
202 time (TE) = 11.5 ms, rare factor = 16, repetition time (TR) = 1200 ms, field of view (FOV) =
203 4x2.6x1.3 cm, matrix = 192x128x64), (2) 3-dimensional T_1 –weighted (fast low angle shot, FLASH,
204 TR= 75 ms, TE= 12 ms, flip angle 15 deg, FOV = 4x2.6x1.3 cm, matrix = 400x260x130), (3) T_1 map
205 (RARE with variable TR (TR=112/227/402/603/837/1118/1470/2655/ 4194/8000 ms, TE=8.7 ms ,
206 rare factor =2, 4 axial slices, FOV= 3.5x3.5 cm, matrix 128x128) and (4) T_2 map (Multi slice multi-
207 echo (MSME) sequence with array of 10 echo times starting from 12ms and equally spaced by 12 ms,
208 TR= 2856 ms, 8 axial slices, FOV=2.5 x 2.5 cm, matrix 256 x 256). For DCE MRI a 3-dimensional
209 T_1–weighted sequence was used (FLASH, TR= 75 ms, TE= 12 ms, flip angle 15 deg, FOV =
210 4x2.6x1.3 cm, matrix = 400x260x130) with 15 repetitions (1 min per repetition). The contrast agent
211 (75 µl of 0.05 mmol/ml meglumine gadoterate, Gd-DOTA; Guerbet, Cadoli, Brussels, Belgium)
212 chased with 100 μl saline, both heated to 37 °C, was manually injected via a catheter placed in a tail
213 vein after 5 min.
214 Data acquisition and processing of T_1 maps was carried out using Paravision 5.1 (Bruker Biospin) and
215 DCE data were analyzed using dedicated software (DCE@urLab v1.0,
216 http://www.die.upm.es/im/archives/DCEurLAB/ [18]). Average dynamic profiles for each time point

were determined based on manual delineation of the most apparent contrast-enhanced zone and similar contralateral region. T2 maps were generated by fitting voxelwise the 10 echoes (12, 24, 36, 48, 60, 72, 84, 96, 108 and 120 ms) to a mono-exponential function (eq.1) with a fit goodness R^2>0.99 (ImageJ, http://rsb.info.nih.gov/ij/ [19]).

Eq.1 $M = M_0 e^{-TE/T_2}$

M: voxel intensity

TE: echo time

T_2: transverse relaxation time

M_0 : initial transverse magnetization

Each map was then smoothed by a median filter with a kernel of 136 μm. Local T2 values were extracted by placing regions of interest of 13 mm^2 centered to the site of injection and on the adjacent slices.

3. Results

a. Longitudinal study of LPS model: microPET, *in vitro* autoradiography and IHC

i. Longitudinal microPET study

A longitudinal microPET study with [^{18}F]DPA-714 was performed to follow up TSPO expression at 1, 3, 7 and 30 days after LPS injection. Analysis demonstrated that the right striatum in which LPS was injected showed higher uptake than the left striatum. Binding potentials calculated with SRTM are presented in table 1 ($BP_{right\ to\ left}$ of animals from the combined MRI-PET study are included in table 1 as the PET scans were performed at the same time points). Statistical calculations proved a significant difference between 1 and 3, 1 and 7, 3 and 30, 7 and 30 days after LPS injection ($P<0.05$). A representative averaged PET image is shown in figure 6b.

Table 1

ii. *In vitro* autoradiography

Analysis of the *in vitro* autoradiography results showed higher tracer uptake in the LPS injected striatum compared to the saline injected striatum. The signal decreased gradually in time with the highest signal at 4 days after LPS injection (figure 2a-c). The right to left ratios at 1, 4, 8 and 31 days after LPS injection were 2.1±0.6, 5.1±1.1, 4.1±0.9 and 3.0±1.1, respectively (figure 1e). Statistical calculations proved a significant difference between 1 and 4, 1 and 8, 4 and 31, 8 and 31 days after LPS injection ($P<0.05$). We performed a blocking study using PK11195 (20 μM) as a blocking agent on brain slices 3 days after LPS injection and PK11195 significantly reduced [^{18}F]DPA-714 binding ($P<0.0001$; figure 2f-g).

Figure 2

iii. Immunohistochemistry (CD68, GFAP and TSPO)

IHC showed immunoreactivity for TSPO and CD68 (a marker of myeloid cells expressed by reactive microglia and macrophages) at 4, 8 and 31 days after LPS injection. The intensity of CD68 immunoreactivity was higher in the ipsilateral than the contralateral hemisphere indicative of microglia activation by LPS. In the ipsilateral striatum, highly CD68+ immunoreactive cells were more abundant at 4 and 8 days and decreased at day 31 (figure 3). Immunoreactivity for TSPO was not detected in the contralateral hemisphere (figure 3f) but was found in the ipsilateral hemisphere located in CD68+ cells (figure 3a-e). Notably, TSPO expression was detected at day 4 and 8 after LPS injection, but not at day 1. At day 31, TSPO staining was still detected but was less prominent than at previous time points after LPS injection. At day 4, TSPO staining was detected in ramified microglia (arrows figure 3a) and in isolated amoeboid cells with macrophage-like morphology (figure 3b) that could correspond to reactive microglia or infiltrated macrophages. TSPO+ cells with amoeboid shape predominated at day 8 (Fig. 3c, d). At day 31, faint TSPO immunoreactivity was detected in ramified CD68+ cells (figure 3e). TSPO immunoreactivity was mainly located in perivascular microglia/macrophages suggesting that the vasculature is a target of the inflammatory reaction after intracerebral LPS administration. In addition, we observed faint TSPO immunoreactivity in regions

surrounding the lesion site (including the corpus callosum and cortical regions) in cells with stellate morphology that could correspond to reactive astrocytes. To confirm this possibility we carried out double immunofluorescence with an antibody against the astroglia marker GFAP (figure 4). While the cells with the highest TSPO immunoreactivity were GFAP negative (figure 4a, c), GFAP positive cells located in the periphery of the LPS injection site showed low TSPO immunoreactivity at days 4, 8 and 31 (figure 4b, d-f) suggesting that reactive astrocytes can express a low level of TSPO.

Figure 3

Figure 4

b. Pre-treatment and displacement microPET study

In order to determine whether *in vivo* binding of [^{18}F]DPA-714 is specific for TSPO and reversible, we performed a pre-treatment study (PK11195 10 mg/kg subcutaneously 60 min before tracer injection; N=3) and a displacement study (PK11195 5 mg/kg intravenously 30 min after tracer injection; N=3) (figure 3). Figure 5a shows a microPET scan at 3 days after LPS injection. The TAC of the pre-treatment study (figure 5b) shows that binding was not blocked completely although there was a decrease in tracer uptake in the LPS injected site compared to the TAC without pre-treatment (figure 3a). IV injection of PK11195 (5 mg/kg) could fully displace the binding of [^{18}F]DPA-714 in the LPS injected site but also in the control (saline injected) site some [^{18}F]DPA-714 binding is displaced (figure 5c).

Figure 5

c. MRI

Considering that tracer uptake may be influenced by BBB integrity, we used DCE MRI to determine the level of BBB breakdown induced by the LPS or saline injection. DCE MRI demonstrated loss of BBB integrity at the LPS injection site but not in the contralateral saline injection site (figure 6a). The contrast enhancement was most apparent at day 1, reduced at day 3 and 7 and not

observable 1 month after LPS injection (figure 7). Accordingly, the differences between the time points for the group averaged DCE MRI signal intensity time profiles from the striatal region with LPS injection showed a similar response. Striatal T2 values of the LPS injected side were higher compared to the contralateral side (saline injected) for each time point with a maximal T2 value reached between 3 and 7 days after LPS injection (figure 8). These data are consistent with the longitudinal PET and autoradiography data.

Figure 6

Figure 7

Figure 8

4. Discussion

This LPS model is a very interesting animal model from a quantification point of view since it has the advantage that neuroinflammation is induced locally around the stereotactic injection site and each animal can be used as its own control using the contralateral hemisphere. *In vivo* PET imaging showed the highest tracer uptake at 3 days after LPS injection and this signal remained quite stable until 7 days after LPS injection. Afterwards, the signal gradually decreased as determined by calculating $BP_{\text{right to left}}$ using the simplified reference tissue model with the contralateral striatum as a reference region (table 1). $BP_{\text{right to left}}$ were also calculated in a slightly different LPS model (unilateral injection of 1-10 μg LPS; saline injected in separate animals as control; different animal strain; LPS from different *E. coli* strains) using [^{18}F]GE-180 and [^{11}C]PK11195 as radioligands by Dickens et al [14]. Additionally, in this study, the animals were scanned at 16 h after LPS injection while the earliest time point in our study was 24 h after LPS injection hampering a reliable comparison of both studies. Interestingly, both studies confirmed an early (16-24 h) increase of TSPO expression after LPS injection. Boutin et al. [6] compared [^{18}F]DPA-714 and [^{11}C]PK11195 in a rat stroke model. Although the BP (calculated with SRTM) seemed comparable for [^{18}F]DPA-714 in both animal models (stroke model: 3.1; LPS model 3.0), the standard deviation was higher for the stroke model (stroke model: 3.0; LPS model 0.3). This variability in animal models of neuroinflammation needs to be considered when comparing different tracers in the same model. Preferably the same animal is scanned with different tracers and the scans need to be performed within a limited time window because of the longitudinal variation in neuroinflammation as observed in this study.

In order to verify specific and reversible binding of [^{18}F]DPA-714 in this specific animal model, displacement and pre-treatment studies were performed. [^{18}F]DPA-714 binding in the lesion site could partly be blocked by pre-treatment with PK11195 (10 mg/kg subcutaneously 60 min before tracer injection). Subcutaneous administration was chosen because of the slow pharmacokinetics and thus slow but rather constant release of the blocking agent in blood. IV injection has fast kinetics but dissociation from the target at the time of tracer injection might occur. Probably the dose administered of PK11195 was not high enough for complete blocking via subcutaneous route. Interestingly, IV

injection (fast pharmacokinetics) of 5 mg/kg PK11195 30 min after tracer injection could fully displace the binding of [^{18}F]DPA-714 in the LPS injected site but also in the saline injected site some [^{18}F]DPA-714 binding is displaced which is probably due to basal TSPO expression in brain. These results are in line with the displacement study performed by Moon et al. in a more comparable LPS model than the LPS model of Dickens et al. (unilateral injection of 50 μg LPS though different rat strain; contralateral striatum as control but no saline injection) using different TSPO tracers ([^{18}F]fluoromethyl-PBR28 and [^{11}C]PBR28), although displacement in non-injected striatum was less than observed in our study [13,14].

In vitro autoradiography showed higher tracer uptake in the LPS injected striatum compared to the saline injected striatum. This higher uptake was already observed at 1 day after LPS injection and increased to the most intense and quite stable signal between 4 and 8 days after LPS injection after which the signal gradually decreased in time as determined by calculating the right to left ratios. The presence of PK11195 (20 μM) completely blocked [^{18}F]DPA-714 binding, suggesting that the observed [^{18}F]DPA-714 binding is TSPO specific. *In vitro* but not *in vivo* retention of [^{18}F]DPA-714 uptake was noticed in white matter (corpus callosum) which was also observed by Dickens et al. using [^{18}F]GE-180 [14].

The *in vitro* data confirmed the *in vivo* data by a positive correlation between $BP_{right\text{-}to\text{-}left}$ (*in vivo* microPET) and right-to-left ratios (*in vitro* autoradiography). Another important validation in pre-clinical PET studies is the confirmation of expression of the target protein by IHC. The purpose of the IHC was the qualitative assessment of TSPO expression and to identify the cells expressing TSPO. TSPO expression at the cellular level was confirmed by IHC using antibodies against TSPO and CD68. CD68 positive myeloid cells were abundant at 4 and 8 days after LPS injection and this reaction was reduced at 31 days. TSPO immunoreactive cells were seen at 4 and 8 days in amoeboid CD68+ cells compatible with reactive microglia or perivascular macrophages. However, at day 4, a comparatively fainter TSPO immunoreactivity was detected in CD68+ ramified microglia cells compatible with early stages of microglia activation. Therefore, these CD68+ reactive ramified microglia cells that were more prominent at day 4 than day 8 could be responsible for the higher

370 [^{18}F]DPA-714 binding found at day 4 compared to day 8 when most TSPO+ cells had amoeboid
371 morphology. The [^{18}F]DPA-714 binding site in the TSPO protein likely differs from the binding sites
372 of the polyclonal anti-TSPO antibody. During the dynamic process of microglia activation, it is
373 possible that the availability of those binding sites changes due to putative interactions of TSPO with
374 other proteins that could mask certain binding sites. Further studies of protein-protein interactions
375 along time might help to elucidate the relevant TSPO binding sites and their availability in relation to
376 the stage of microglial activation. No CD68 or TSPO immunoreactivity was observed in the
377 contralateral site. In addition, we detected faint TSPO immunoreactivity in astrocytes in regions
378 surrounding the injection site, but it is currently unknown whether low TSPO expression in reactive
379 astrocytes contributed to the PET signal.

380 We performed MRI studies to be certain that tracer uptake was not due to BBB disruption but
381 to upregulation of TSPO expression induced by the LPS injection. DCE MRI indicated maximal BBB
382 breakdown at day 1 after LPS injection with progressive restoration and full recovery at 1 month after
383 LPS injection. These data suggest that tracer uptake was due to TSPO binding as no tracer uptake was
384 seen at day 1 after LPS injection when BBB breakdown was at maximum. The fact that *in vivo*
385 microPET data (possible influence of BBB integrity on tracer uptake) and *in vitro* autoradiography
386 data (no influence of BBB on tracer uptake) were positively correlated, suggested tracer uptake during
387 *in vivo* PET imaging was not due to BBB disruption. Conversely, BBB breakdown will favour
388 vascular and perivascular inflammation and might contribute to microglia/macrophage activation
389 around the vasculature. The quantification of the striatal transverse relaxation (T2) showed a nice
390 correlation with the PET and autoradiography imaging suggesting that T2 in this case may reflect the
391 underlying inflammation process.

392 The characterization of the LPS model with an established neuroinflammation tracer is of great
393 importance as we are developing and evaluating new radiotracers for potential new targets upregulated
394 during neuroinflammation. The longitudinal variation in neuroinflammation (as measured in this
395 study) has to be taken into account when comparing different tracers. The LPS model is useful for first
396 screening of newly developed tracers because of the easy design and the robust, unilateral

inflammatory reaction allowing the use of the contralateral region as control. The radioligands with the most potential can be selected for further screening in more clinical relevant disease models accelerating the translation to human PET studies. Additionally, this animal model is suitable to evaluate (new) anti-inflammatory therapy in an initial preclinical setting. This preliminary screening can select the most potential compounds for further evaluation and accelerate the translation of the therapy to humans.

This model will now be used to evaluate radioligands for other targets upregulated during neuroinflammation such as the CB_2 and $P2X_7$ receptor thereby accelerating the PET radioligand development for *in vivo* imaging of neuroinflammation [3].

5. Acknowledgments

Dieter Ory is a fellow of the Research Foundation Flanders (FWO). This research is funded by the European Union's Seventh Framework Programme (FP7/2007-2013) under grant agreement n° HEALTH-F2-2011-278850 (INMiND). Guy Bormans, Tom Dresselaers and Uwe Himmelreich received financial support from the KU Leuven Program Financing IMIR, IWT MIRIAD (SBO 130065) and FWO (FWO: G0B2814N, FWO: KaN 1.5.220.13N). Koen Van Laere is a Senior Research Fellow for FWO. We would like to thank Julie Cornelis, Tinne Buelens and Ann Van Santvoort for their excellent assistance in the animal work and data processing.

6. References

[1] Jacobs AH, Tavitian B. Noninvasive molecular imaging of neuroinflammation. J Cereb Blood Flow Metab 2012;32:1393–415.

[2] Papadopoulos V, Baraldi M, Guilarte TR, Knudsen TB, Lacapère J-J, Lindemann P, et al. Translocator protein (18kDa): new nomenclature for the peripheral-type benzodiazepine receptor based on its structure and molecular function. Trends Pharmacol Sci 2006;27:402–9.

[3] Ory D, Celen S, Verbruggen A, Bormans G. PET Radioligands for In Vivo Visualization of Neuroinflammation. Curr Pharm Des 2014;20:5897–913.

[4] Bae K-R, Shim H-J, Balu D, Kim SR, Yu S-W. Translocator protein 18 kDa negatively regulates inflammation in microglia. J Neuroimmune Pharmacol 2014;9:424–37.

[5] Chen M-K, Guilarte TR. Translocator protein 18 kDa (TSPO): molecular sensor of brain injury and repair. Pharmacol Ther 2008;118:1–17.

[6] Boutin H, Prenant C, Maroy R, Galea J, Greenhalgh AD, Smigova A, et al. [18F]DPA-714: direct comparison with [11C]PK11195 in a model of cerebral ischemia in rats. PLoS One 2013;8:e56441.

[7] Chauveau F, Van Camp N, Dollé F, Kuhnast B, Hinnen F, Damont A, et al. Comparative evaluation of the translocator protein radioligands 11C-DPA-713, 18F-DPA-714, and 11C-PK11195 in a rat model of acute neuroinflammation. J Nucl Med 2009;50:468–76.

[8] Harhausen D, Sudmann V, Khojasteh U, Müller J, Zille M, Graham K, et al. Specific imaging of inflammation with the 18 kDa translocator protein ligand DPA-714 in animal models of epilepsy and stroke. PLoS One 2013;8:e69529.

[9] Arlicot N, Vercouillie J, Ribeiro M-J, Tauber C, Venel Y, Baulieu J-L, et al. Initial evaluation in healthy humans of [18F]DPA-714, a potential PET biomarker for neuroinflammation. Nucl Med Biol 2012;39:570–8.

[10] Corcia P, Tauber C, Vercoullie J, Arlicot N, Prunier C, Praline J, et al. Molecular imaging of microglial activation in amyotrophic lateral sclerosis. PLoS One 2012;7:e52941.

[11] Owen DR, Yeo AJ, Gunn RN, Song K, Wadsworth G, Lewis A, et al. An 18-kDa translocator protein (TSPO) polymorphism explains differences in binding affinity of the PET radioligand PBR28. J Cereb Blood Flow Metab 2012;32:1–5.

[12] Glass CK, Saijo K, Winner B, Marchetto MC, Gage FH. Mechanisms underlying inflammation in neurodegeneration. Cell 2010;140:918–34.

[13] Moon BS, Kim BS, Park C, Jung JH, Lee YW, Lee H-Y, et al. [(18)F]Fluoromethyl-PBR28 as a potential radiotracer for TSPO: preclinical comparison with [(11)C]PBR28 in a rat model of neuroinflammation. Bioconjug Chem 2014;25:442–50.

[14] Dickens AM, Vainio S, Marjamäki P, Johansson J, Lehtiniemi P, Rokka J, et al. Detection of microglial activation in an acute model of neuroinflammation using PET and radiotracers 11C-(R)-PK11195 and 18F-GE-180. J Nucl Med 2014;55:466–72.

[15] Damont A, Hinnen F, Kuhnast B, Schöllhorn-Peyronneau M, James M, Luus C, et al. Radiosynthesis of [18 F]DPA-714, a selective radioligand for imaging the translocator protein (18 kDa) with PET. J Label Compd Radiopharm 2008;51:286–92.

[16] Casteels C, Vermaelen P, Nuyts J, Van Der Linden A, Baekelandt V, Mortelmans L, et al. Construction and evaluation of multitracer small-animal PET probabilistic atlases for voxel-based functional mapping of the rat brain. J Nucl Med 2006;47:1858–66.

[17] Lammertsma AA, Hume SP. Simplified reference tissue model for PET receptor studies. Neuroimage 1996;4:153–8.

[18] Ortuño JE, Ledesma-Carbayo MJ, Simões R V, Candiota AP, Arús C, Santos A. DCE@urLAB: a dynamic contrast-enhanced MRI pharmacokinetic analysis tool for preclinical data. BMC Bioinformatics 2013;14:316.

[19] Abramoff M, Magalhaes P, Ram S. Image processing with ImageJ. Biophotonics Int 2004:36–42.

TABLES

TABLE 1: Kinetic modeling. Binding potential ± SD in right striatum obtained by SRTM with left striatum as reference tissue

Left striatum as reference tissue				
Days after LPS injection	1 (n=3)	3 (n=5)	7 (n=4)	30 (n=3)
Binding potential	0.4 ± 0.1	3.0 ± 0.3	2.5 ± 0.6	0.9 ± 0.2

FIGURE CAPTIONS

FIGURE 2. Experimental design. Following experiments were performed**:** 1 day after LPS injection, microPET (n=3), MRI (n=6), *in vitro* autoradiography and IHC (n=3); 3 days after LPS injection microPET (n=5) and MRI (n=5); 4 days after LPS injection, *in vitro* autoradiography and IHC (n=3); 7 days after LPS injection, microPET (n=4) and MRI (n=6); 8 days after LPS injection, *in vitro* autoradiography and IHC (n=4); 30 days after LPS injection, microPET (n=3) and MRI (n=4); 31 days after LPS injection, *in vitro* autoradiography and IHC (n=4). ARX: *in vitro* autoradiography; IHC: immunohistochemistry

FIGURE 2. *In vitro* autoradiography of brain slices of rat LPS model using [^{18}F]DPA-714. Transversal brain sections made of rats, respectively 4 days (a), 8 days (b) and 31 days (c) after LPS injection, incubated with [^{18}F]DPA-714. LPS was injected in the right striatum and the LPS-induced TSPO expression is clearly visualized by [^{18}F]DPA-714. [^{18}F]DPA-714 binding could be blocked with 20 μM PK11195 3 days after LPS injection (> 96%) (d-e). The signal is the highest in the LPS injected striatum 4 days after LPS injection and the right to left (R/L) ratio decreases gradually in time (f).

FIGURE 3. IHC on LPS model: TSPO and CD68. TSPO is expressed in CD68+ reactive microglia/macrophages. Images show TSPO (green), CD68 (red), the nuclei labelled with TO-PRO3 (blue), and the merged staining in sections taken from the ipsilateral hemisphere at day 4 (a, b), 8 (c,d) and 31 (e) after LPS administration. TSPO is mostly expressed in CD68+ cells in the ipsilateral hemisphere (arrows in a-e) but is not detected in the contralateral hemisphere (f). Bar scale: 10 μm.

FIGURE 4. IHC on LPS model: TSPO and GFAP. Faint TSPO expression is observed in reactive astrocytes. Images show TSPO (green), GFAO (red), the nuclei labelled with TO-PRO3 (blue), and the merged staining in sections taken from the ipsilateral hemisphere at day 4 (a, b), 8 (c-e) and 31 (f) after LPS administration. Cells strongly immunoreactive for TSPO are not GFPA positive (arrows in a-c). However, reactive astrocytes located at the periphery of the injection site in the ipsilateral hemisphere show a faint TSPO immunoreactivity 8 and 31 days after LPS administration (arrows in d-f). Bar scale: 10 μm.

FIGURE 5. MicroPET studies with [^{18}F]DPA-714 in a LPS rat model. a: TAC of a microPET scan at 3 days after LPS injection; b: TAC of a microPET study after pre-treatment with PK11195 (subcutaneously 10 mg/kg 60 min before tracer injection) at 3 days after LPS injection; c: TAC of a displacement microPET study with PK11195 (intravenously 5 mg/kg 30 min after tracer injection) at 3 days after LPS injection. Animals were kept under gas anesthesia (2.5% isoflurane in O_2 at a flow rate of 1 L/min). Rats were injected with about 74 MBq of [^{18}F]DPA-714 via a tail vein.

FIGURE 6. *In vivo* DCE MRI and microPET study of one representative animal in time. a: dynamic signal intensity (SI) changes from the LPS or saline injection zones. BBB disruption near the LPS injection site (right hemisphere) is evident at 1 day and reduced at 3 and 7 days. No contrast enhancement is seen 1 month after the LPS injection or near the saline injection site (left hemisphere; all time points). b: averaged microPET images of the whole scan (120 min) after [^{18}F]DPA-714 injection were acquired. Data were normalized for injected activity and body weight of the animal (SUV). Animals were kept under gas anesthesia (2.5% isoflurane in O_2 at a flow rate of 1 L/min). Rats were injected with about 74 MBq of [^{18}F]DPA-714 via a tail vein.

FIGURE 7. *In vivo* DCE MRI. Dynamic signal intensity (SI) changes from the LPS or saline injection zones resulting from the Gd-DOTA injection at the different time points 1 day, 3 days, 1 week and 1 month. a: BBB disruption near the LPS injection site (right hemisphere) is present at 1, 3 and 7 days. b: No contrast enhancement is seen at 1 month after the LPS injection or near the saline injection site (left hemisphere; all time points; CA: contrast agent).

FIGURE 8. Parametric T2 maps. a: Parametric T2 maps at day 1, 3, 7 and 30 of a representative animal with injection of 50 μg LPS in the right striatum (white arrow) and saline on the left side. T2 maps are all scaled from 30 to 70 ms. b: Striatal T2 values, data are expressed as mean ± SD. Day 1: N = 3, Day 3: N = 5, Day 7: N = 6, Day 30: N = 5.

Figure 1
Click here to download high resolution image

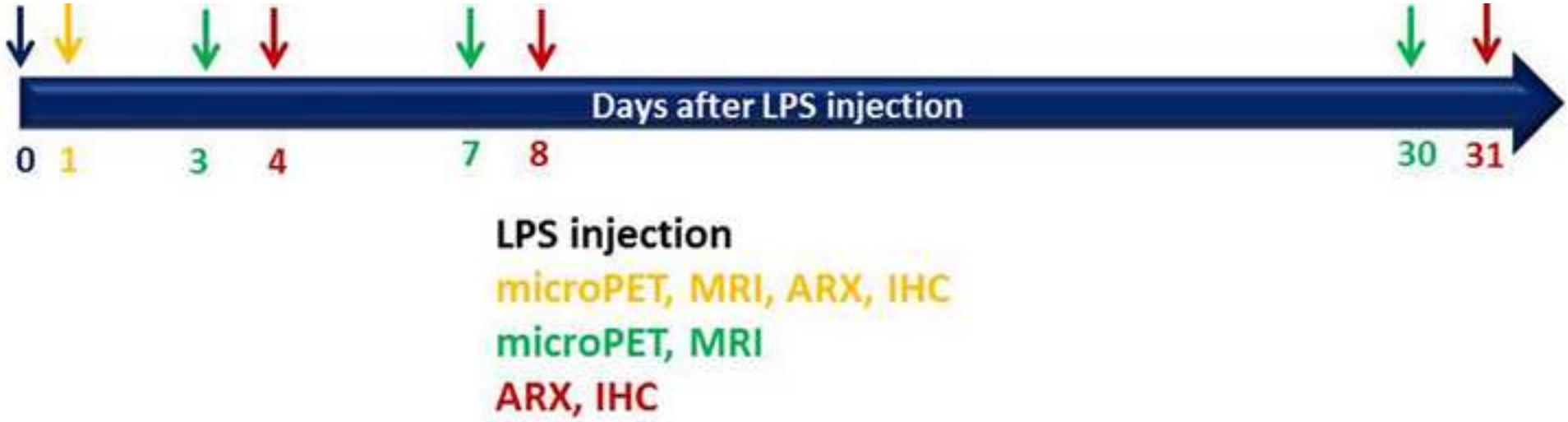

Figure 2

Click here to download high resolution image

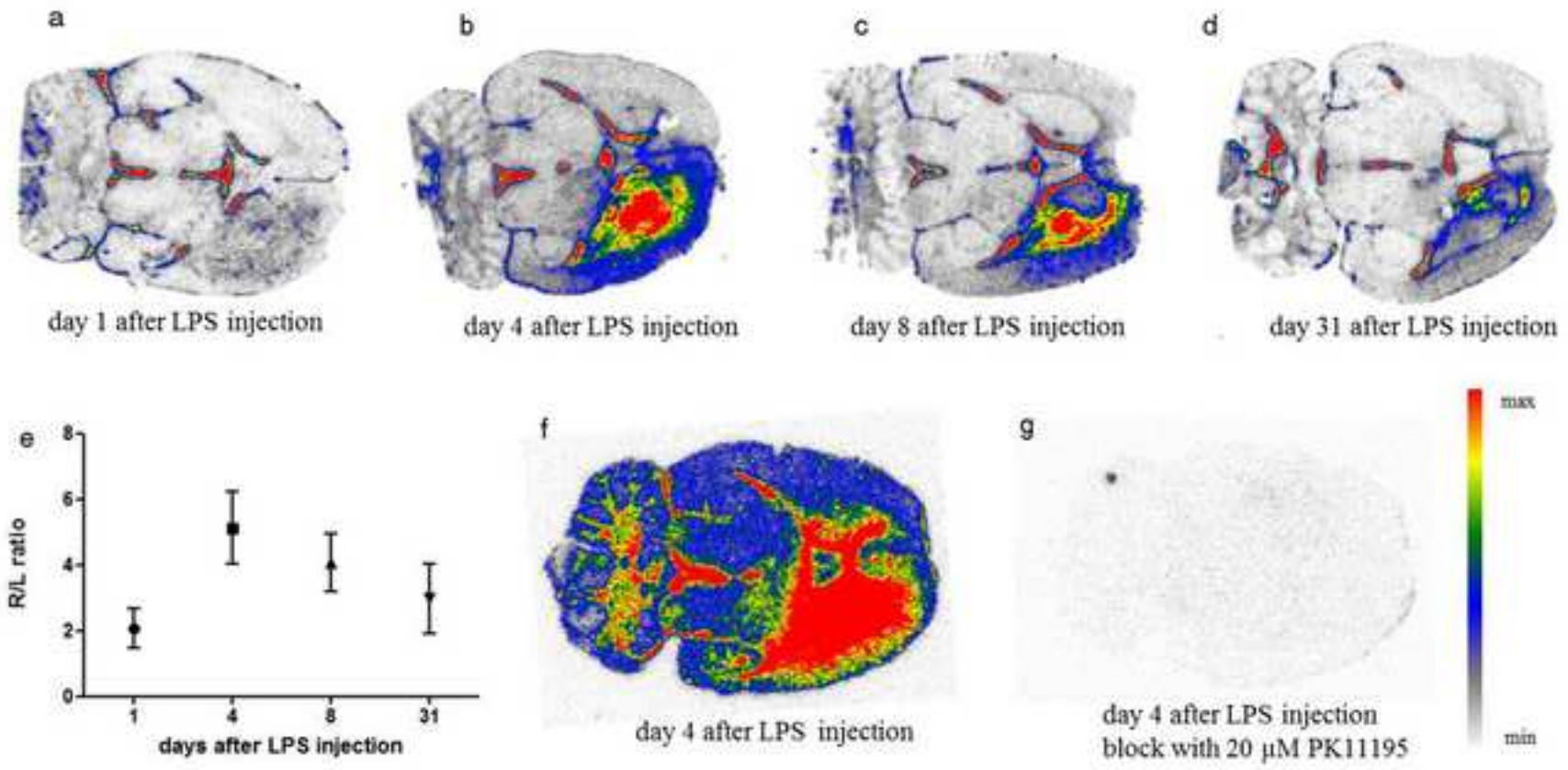

Figure 3

Click here to download high resolution image

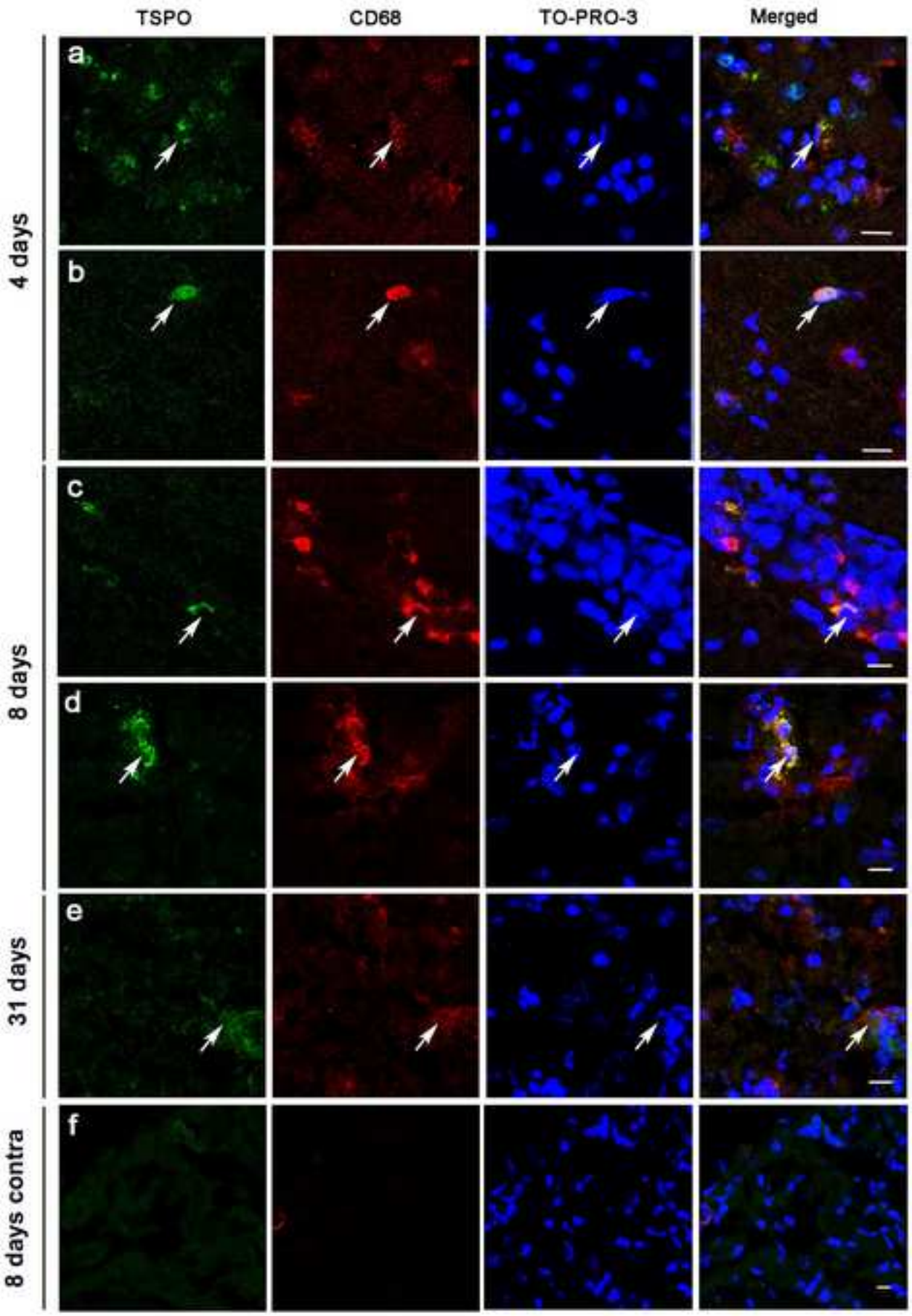

Figure 4

Click here to download high resolution image

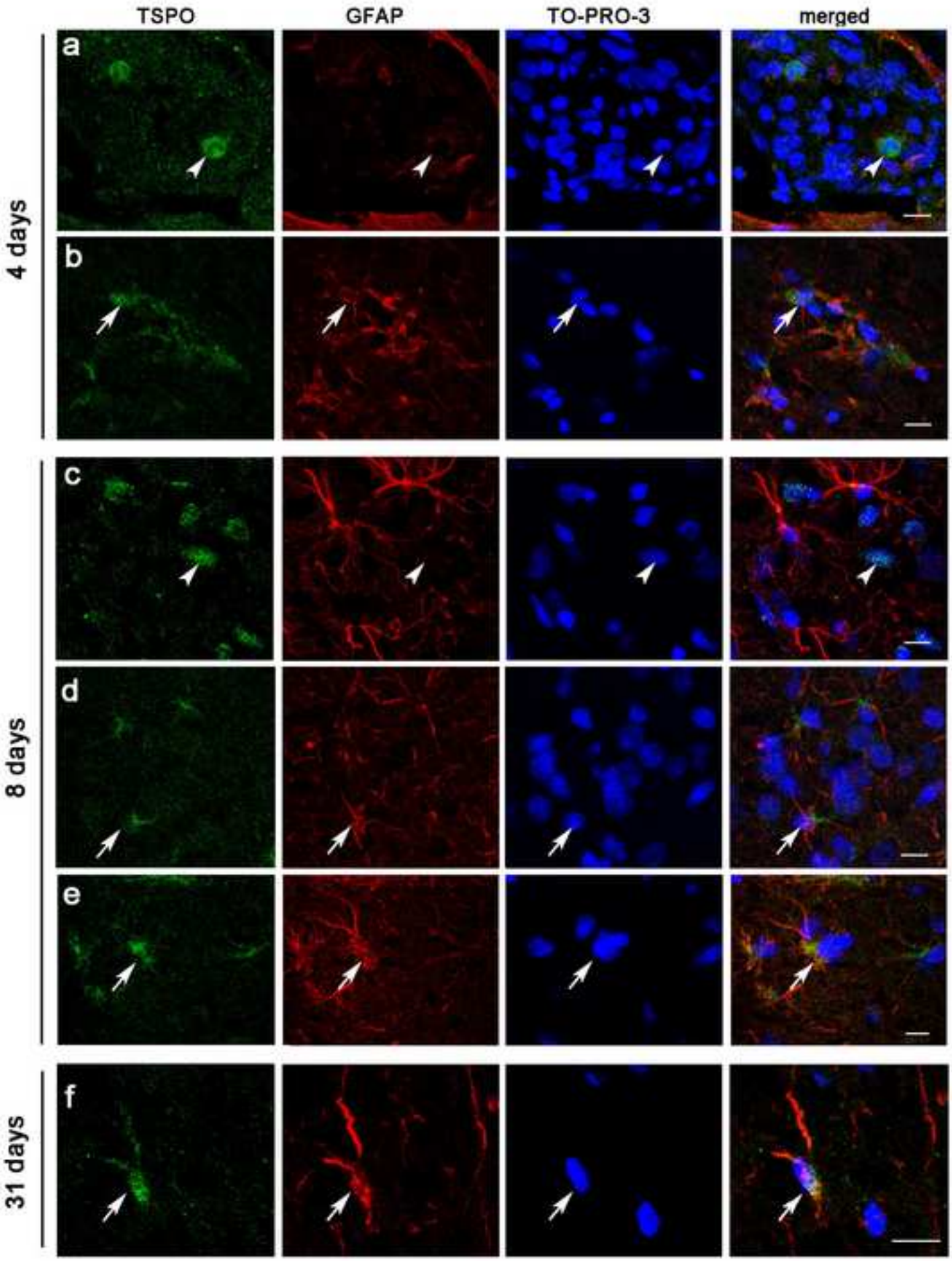

Figure 5

Click here to download high resolution image

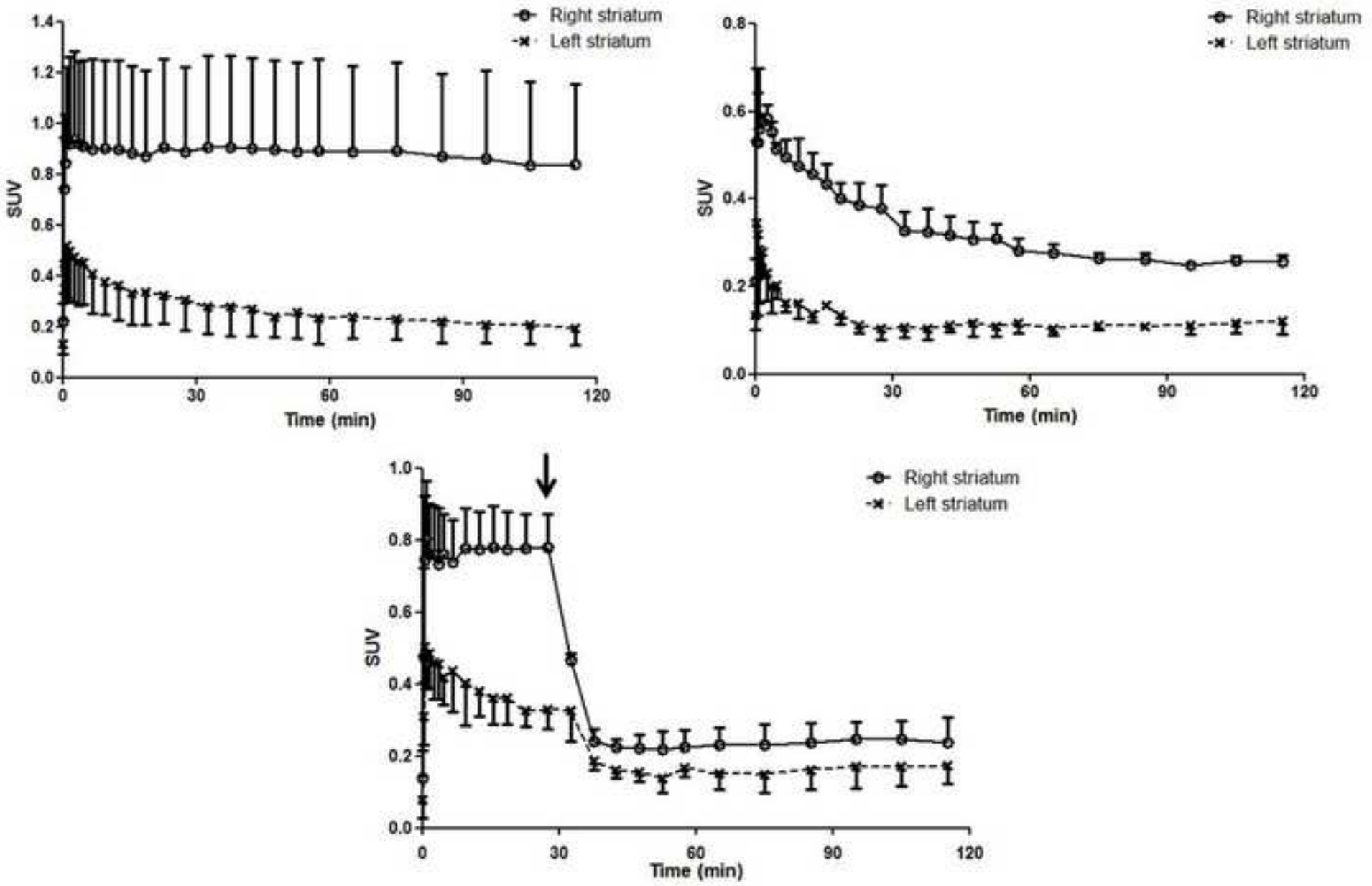

Figure 6

Click here to download high resolution image

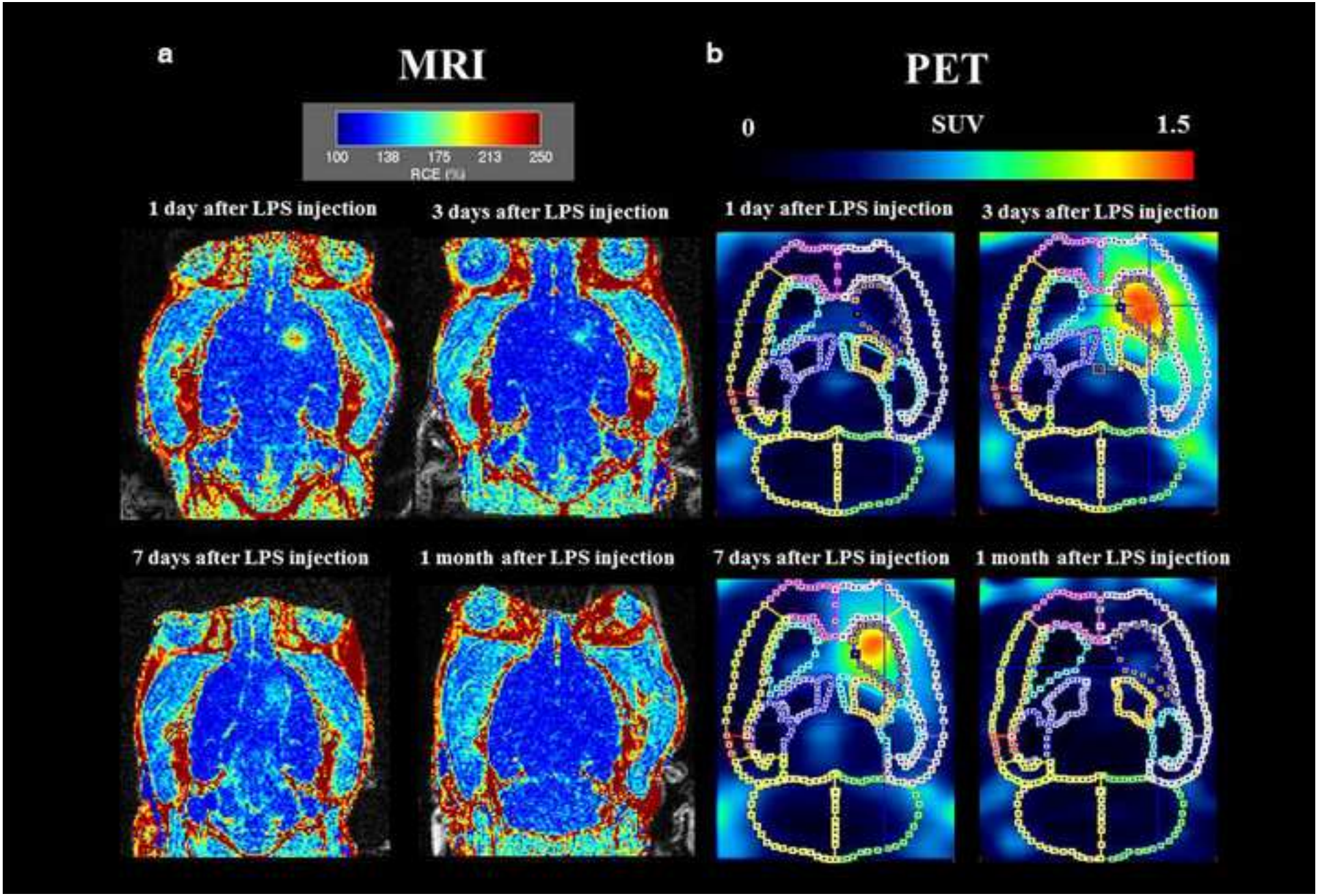

Figure 7

Click here to download high resolution image

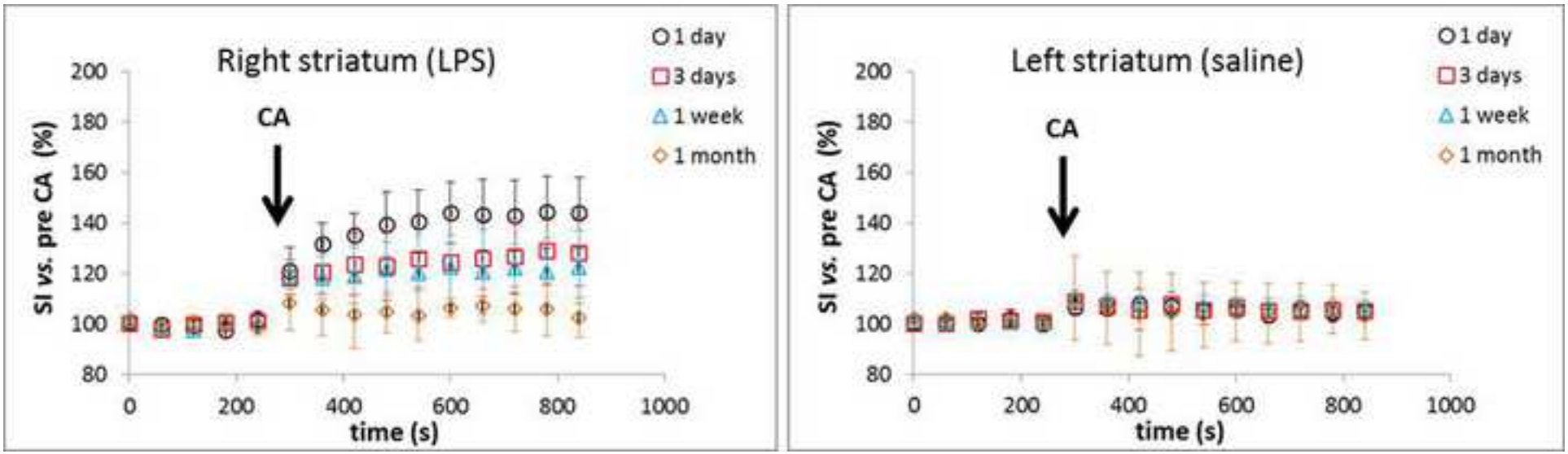

Figure 8

Click here to download high resolution image